Experimental assessment of multi-phase flow distribution in an evaporator header through Design of Experiments techniques

Tempesti, Claretta; Lecardonnel, Aude; Laboureur, Delphine

DOI
10.1016/j.expthermflusci.2024.111359

Publication date
2025

Document Version
Final published version

Published in
Experimental Thermal and Fluid Science

Citation (APA)
Tempesti, C., Lecardonnel, A., & Laboureur, D. (2025). Experimental assessment of multi-phase flow distribution in an evaporator header through Design of Experiments techniques. *Experimental Thermal and Fluid Science*, *162*, Article 111359. https://doi.org/10.1016/j.expthermflusci.2024.111359

Experimental Thermal and Fluid Science 162 (2025) 111359

Contents lists available at ScienceDirect

Experimental Thermal and Fluid Science

journal homepage: www.elsevier.com/locate/etfs

Experimental assessment of multi-phase flow distribution in an evaporator header through Design of Experiments techniques

Claretta Tempesti [a,*], Aude Lecardonnel [a,b], Delphine Laboureur [a]

[a] Von Karman Institute for Fluid dynamics, Chaussee de Waterloo 72, Rhode-Saint-Genese, 1640, Belgium
[b] Propulsion and Power, Delft University of Technology, Kluyverweg 1, Delft, 2629HS, The Netherlands

ARTICLE INFO

Keywords:
Design of experiment
Applied statistical data analysis
Experimental
Evaporator
Two-phase flow

ABSTRACT

The uneven distribution of flow phases in evaporator channels can drop the heat exchanger efficiency up to 30%. Due to its dependence on the interaction of several coexisting variables – both geometry, operating conditions, and fluid properties – it is a complex phenomenon to analyze. Most studies focus on the effect of single parameters: this is an inefficient and expensive way of doing experiments, and the results lack in understanding how the combination of variables affects the flow distribution. This paper presents a methodology to optimally characterize and predict the distribution of flow phases in the channels of an evaporator header based on Design of Experiment (DoE) techniques. Despite the proven potential of DoE methods, they have never been applied in this field. Tests were conducted with an air–water mixture in the configuration horizontal header with vertical channels with downward flow, varying inlet pipe position, channels intrusion, presence of a splashing grid at the header inlet, and air and water flow rates. Results prove that, when working with complex processes, interaction effects between variables cannot be neglected as they significantly affect the response. The most affecting parameter was found to be the air flow rate, followed by the combination between inlet pipe position and presence of the splashing grid. With horizontal inlet, the optimal response was given by absence of intrusion, presence of the splashing grid, lowest water, and highest air flow rate. Instead, for the vertical case, the distribution was enhanced with the highest intrusion, absence of the grid, and highest water and air flow rates. Lastly a first attempt to model the process was performed. Even if a universal regression model has low accuracy (51%), restricting the area of analysis can result in valid predictive relations, with accuracies up to 91.4%.

1. Introduction

Vapor cycle systems are in charge of equipment cooling and environmental control systems in the aviation sector. Among their components, evaporators have a significant influence on the overall performance, and their optimization still has room for improvement. This is due to the coexistence of different flow phases, which (a) makes it a complex phenomenon to fully characterize and (b) strongly affects the efficiency. Indeed, the uneven distribution of flow phases in evaporator channels can drop the heat exchanger performances by 13% [1,2] and up to 30% in extreme cases [3]. The major challenge lies in the fact that the prediction of the two-phase flow distribution strongly depends on a wide number of parameters of different nature, from fluid properties, to geometry, to operating conditions. Therefore, considerable research effort has been devoted to its characterization and prediction in the past decades. Several major authors have experimentally contributed to improve the understanding of the impact of various parameters. Other authors have contributed by producing exhaustive reviews about the progresses and main findings in the field of two-phase flow maldistribution [4,5]. One can cite the work of Kim et al. [6,7] that tried to assess the impact of inlet and outlet tube directions, and of the channels protrusion depth in a cylindrical header connected to 10 or 30 flat channels using an air/water mixture. They studied a Horizontal Header with Vertical Downward (HH-VDC) and Vertical Upward (HH-VUC) channels. However, only the annular flow pattern was analyzed. Their main finding for the HH-VCD was that the water flow distribution was impacted by the tube protrusion as it helps the water phase to reach the rear part of the header. Increasing mass flux and quality led to a similar effect. However, for the HH-VUC all these parameters were not found to have a significant impact on the flow distribution. Similarly, a parallel inlet/outlet or a reverse inlet/outlet tube direction did not affect the water distribution. When studying the inlet direction, the vertical one yielded the best distribution observed, followed by the

* Correspondence to: Università degli Studi di Firenze, Dipartimento di Ingegneria Industriale (DIEF), Via Santa Marta 3, 50139 Firenze, Italy.
E-mail address: claretta.tempesti@unifi.it (C. Tempesti).

https://doi.org/10.1016/j.expthermflusci.2024.111359
Received 21 August 2024; Received in revised form 25 October 2024; Accepted 14 November 2024
Available online 22 November 2024

normal inlet and finally by the parallel inlet. Kim et al. also studied the distribution of R-410a flow inside a multiparallel channel evaporator similar to the design of their previous study [8], but with a vertically oriented header. They focused on the outlet location impact, concluding that the bottom configuration led to a better distribution. The findings of Zou et al. [9] a few years later highlighted the importance of the fluid property and especially the phase density ratio. They conducted a study on a vertical header linked to five horizontal channels with two passes, examining four refrigerants: R245fa, R134a, R410 A, and R32. They visualized the two-phase flow behavior within the header and compared the distribution of liquid flow within the five channels of the second pass to gain insights into how fluid properties affect two-phase flow distribution. They deduced that the disparity between the densities of the liquid and vapor phases was crucial for the two-phase flow distribution as it significantly influenced the inertial forces. This is in line with the more recent findings from the work of Razlan et al. [10]. They compared the two-phase flow patterns of an air/water mixture and a R134a flow inside the header of a multiple parallel channel simplified evaporator. They found that for the equal liquid and gas superficial velocities, different flow patterns are obtained between the air/water and the R134a. This led to different flow distributions among the channels. Over a decade, J. K. Lee et al. investigated the behavior of an air/water mixture in all five possible header and channel orientations: Horizontal Header with Vertical Upward and Downward (HH-VUC and HH-VUD) Channels [11], Vertical Upward and Downward Header with Horizontal Channels (VUH-HC and VDH-HC) [12–14], and Horizontal Header with Horizontal Channels (HH-HC) [11,15]. Their research underscored the typical behavior of both liquid and vapor phases for each of the five orientations. This behavior, and consequently the two-phase flow distribution, seemed to be heavily reliant on the orientation of the header and channel as the effect of gravity varies greatly with the direction of the flow. They also discovered that the optimal intrusion depth is 1/8 of the header hydraulic diameter for a vertical upward header with horizontal channels. Dario et al. [16] carried out a similar study on the impact of the header and channel orientation, arriving at similar conclusions. However, they also examined the effect of the inlet position for each orientation with an air/water mixture in atmospheric conditions. They concluded that for a horizontal header, an inlet pipe perpendicular to both the header and the channels is more favorable than an inlet perpendicular to the header but parallel to the channels. For a vertical downward header, they were unable to identify an inlet position that enhanced the uniformity of the liquid distribution. Fei et al. [17] analyzed the behavior of R134a two-phase flow within a horizontal header connected to five vertical downward channels. They altered the inlet quality and the mass flux and observed their effects on the flow pattern at the header entrance, as well as their impact on the flow distribution among the channels. Depending on the tested inlet quality and flow velocity, the inlet flow structure ranged from a stratified condition to three different intensity liquid jets and, finally, a mist flow. They reported that the best distribution was achieved when a mist flow condition was reached. Ahmad et al. [18] conducted a similar study on the two-phase flow behavior of HFE 7100 inside a horizontal header connected to eight vertical upward, vertical downward, and horizontal channels. They reported flow structures at the header inlet for a horizontal header and vertical downward channels comparable to those of Fei et al. [17], but the transitions occurred under different inlet conditions. Generally, they observed that an increase in the momentum of the two-phase flow, particularly of the liquid one, improved the distributions of both the liquid and vapor phases. This is in line with the more recent work from Redo et al. [19]. They studied the distribution of R410 A inside horizontal microchannels connected to a vertical upward header for various mass flow rates and quality, and for tube protrusions of 0% and 50%. They observed that an increase in the inertial forces of the two-phase flow improves the distribution.

Despite the substantial work on two-phase flow maldistribution over the past decades, these studies have significant limitations and it is still not possible to draw exact conclusions. Overall, experimental studies indicated that the phenomenon depends on the interaction of several coexisting factors. However, most studies are focused on the effect of single variables for a specific flow orientation (i.e. vertical or horizontal) and for water-steam or water-air mixtures [20], which does not accurately represent the actual properties of the liquid and vapor phases of refrigerants. Furthermore, quantifying maldistribution experimentally is challenging, and tests are often conducted on simplified geometries. Studies like the ones mentioned above typically use experimental methods relying on liquid and vapor phase separation after each evaporator channel. Such methods do not enable continuous experimental tests and are therefore highly cumbersome. In addition, they follow the so-called one-factor-at-a-time (OFAT) strategy, which consists of varying each parameter over its full range individually, while the others are held constant. This is an inefficient and expensive way of doing experiments. Moreover, the optimal configuration of variables identified with OFAT methods could not be the best, as the result fails to consider any possible interaction between the parameters [21], which may lead to erroneous results. In this context, the use of Design of Experiments (DoE) techniques fits perfectly. The advantages of these methods rely on the ability to assess how individual parameters and their combination affect the response while minimizing the number of tests needed. They provide practical guidance to experimentalists for the definition of the test matrix reducing the number of runs required and for analyzing the results with statistical methods, resulting in valid and objective conclusions [21]. Details about the theory underlying DoE techniques are explained in Section 2.

Despite the potentiality of DoE methods, they have poor diffusion in research activities and are mainly applied in the industrial sector. In multi-phase flows sector, some applications were found in the state of the art. Kim et al. [22] applied fractional factorial design to improve the hydrodynamic performances of a multi-phase pump for an offshore oil plant. The authors were able to select the design variables with stronger effects, which were then used to generate an optimized model using the response surface method (RSM). Bozzini et al. [23], evaluated the effects of key operating parameters – fluid flow velocity, particle mass flow rate, and phase volume ratio – in erosion–corrosion damaging phenomena with multi-phase flows. The process analyzed in this paper is affected by a huge amount of parameters, including flow conditions, composition of the structural material, chemistry of the flowing system, and temperature. The application of a design of experiments approach allowed to evaluate single and joint effects of the simulation parameters on the overall damage, identifying the order of importance of the variables tested. Capetillo et al. [24], applied a Full Factorial method to identify the impact of three injection parameters – injection velocity, spray angle, and droplet size – on the performance of a selective catalytic reaction (SCR) system in automotive application. The authors found that for the operation point under analysis, only injection velocity and spray angle had a significant impact on the performance. Having applied Full Factorial design, they were able to capture with fine details also second order interactions between variables. Based on these DoE results, they employed a linear regression model and developed a series of response surfaces, which can be used as guidance for future SCR system designs towards desired performances. In evaporator applications, Sung et al. [25] used Taguchi DoE methodology to determine the optimal design parameters of a micro evaporator. Geometric parameters – number of lateral gaps, channel width, and lateral gap size – were varied to maximize the heat transfer coefficient, and the most sensitive variable was found to be the channel width. According to these authors, the application of DoE techniques is a good approach for case studies where the phenomena under investigation are difficult to define theoretically.

Despite being applied to different research fields, what is common to all these cited studies is the complexity of investigation, due to the coexistence of various physical phenomena which affect the response. Indeed, the presence of multi-phase flows increases the complexity and

Table 1
Example of a designed experimental matrix. L_1 and L_2 indicate the different levels of the 3 factors.

Run	Factors			Response
	x_1	x_2	x_3	
1	L_1	L_1	L_1	y_1
2	L_2	L_1	L_1	y_2
3	L_1	L_2	L_1	y_3
4	L_2	L_2	L_1	y_4

modeling of processes, as it causes the involvement and dependence on a huge number of parameters of different nature. For these cases, the application of different DoE methods can help in all phases of research, from planning to analysis of results.

To the authors' knowledge, there are no existing studies in literature that applied DoE methods for the specific application contained herein. This paper presents the development of a methodology to optimally characterize and predict the distribution of flow phases in the channels of an evaporator header based on DoE techniques. Its usage can generate two advantages: (1) assess the effect of the combination of all the desired parameters on the flow distribution, and (2) reduce to the minimum the required tests. The developed methodology was then applied to a specific test case to prove its validity. Both the definition of the test matrix and the analysis of the experimental results were defined based on DoE theory. It is a novelty in this field and it can give insights into the phenomena that remain usually hidden when OFAT methods are used. The paper is structured as follows: Section 2 introduces the theory underlying DoE methods and Section 3 defines with detail all the variables tested, the experimental set-up, and the acquisition system. Section 4 describes the definition of the experimental matrix with DoE techniques. Lastly, Section 5 shows the results, and Section 6 draws the main conclusion of the analysis.

2. Design of experiment

Design of Experiments is a systematic, efficient method for planning an experimental campaign. It serves to understand how multiple input parameters (called **factors**) and their interactions affect the response. The output obtained is displayed as a matrix, which defines, for every experiment, the **level** to be tested for each factor, i.e. the value of each parameter. Table 1 shows an example with four runs and three two-level factors. Well-chosen experimental designs *maximize the amount of "information" that can be obtained for a given amount of experimental effort* [26]. DoE techniques reduce the number of experiments required and analyze the results by statistical methods, resulting in valid and objective conclusions [21], saving resources and reducing costs.

Process modeling, which underlies DoE, allows to describe the variation of a response variable y by means of a mathematical function of one or more other quantities $f(\vec{x}, \vec{\beta})$, and a random component ϵ:

$$y = f(\vec{x}, \vec{\beta}) + \epsilon \tag{1}$$

Here $(x_1, x_2, \dots, x_n)$ are the factors varied during the campaign, $(\beta_1, \beta_2, \dots, \beta_n)$ are the quantities that will be estimated during the data analysis and ϵ is the error. For example, a linear model with two factors, x_1 and x_2, can be written as:

$$y = \beta_0 + \beta_1 x_1 + \beta_2 x_2 + \beta_{12} x_1 x_2 + \epsilon \tag{2}$$

Here, the second and third terms on the right hand side are the **main effect terms**, and the fourth one is the **two-way interaction term**. Clearly, a full model could include many cross-products or interaction terms. However, in the majority of cases, they are not included, as they give few additional information but require an exponentially increased number of tests.

In DoE applications, the set of $\vec{x}$ values to be tested, i.e. the combination of factor levels, can vary from one design to another based on what the campaign is focused on. For each specific application, some distributions of data in the $\vec{x}$ vector may yield better coefficient estimates (with minimal variation) than others. In the extreme case, with the so-called "Full Factorial Design", every combination of factor levels is analyzed within the experimental space. It is an expensive method, but it allows to capture high-order interactions with great detail, providing the most comprehensive insight into the system's behavior [27]. When the number of variables involved is too high to run a Full Factorial Design, different DoE techniques can be applied to reduce the set of values to be tested, running only a fraction of the complete factorial. Time and resources needed decrease at the expense of less detailed information on the process. A visual example is given in Fig. 1, where the design space of a 2-factor 2-level system is drawn for a Full Factorial and for a Fractional Factorial.

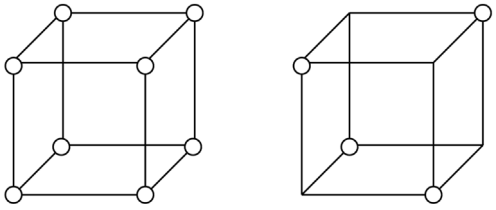

Fig. 1. Design space of a Full Factorial of Fractional Factorial with 2 levels and 2 factors.

Selecting the optimal design means identifying the best way to sample the space domain. In order to do it, there are clearly defined tasks that should be followed:

1. Phase 1: problem layout.
   (a) Recognition and statement of the problem;
   (b) Choice of factors, levels and level ranges;
   (c) Selection of the response variable;
2. Phase 2: definition of experimental matrix.
   (a) Choice of DoE method for the planning of the test campaign;
3. Phase 3: test conduction and analysis.
   (a) Conduction of the experiments;
   (b) Statistical analysis of results.

The first phase involves the definition of the objectives and of the parameters in charge. Depending on these two aspects, various existing DoE techniques can be selected. The heart of the process lies in the second Phase, i.e. in the choice of the DoE method that gives the best combination of factor levels to be tested for the specific application and aim of the campaign. The objective of the experiments could be choosing between two alternatives (with which *comparative designs* should be applied), selecting key factors that affect the response (with *screening experiments*), or even modeling and optimizing a process (with *response surface designs*) [26]. In the early stages of experimentation the analysis is usually exploratory, aiming at identifying important sources of variability and ranking the order of importance of the factors tested. Subsequently, the analysis can be confirmatory, for example to evaluate the effect of the most affecting variables in a narrower range. Lastly, in some cases a mathematical model of the response can be developed [28].

Given the multitude of different DoEs that can theoretically match the type of investigation, it is not straightforward to identify which design provides the best possible insight using the least resources. At the same time, existing designed matrixes have always strict constraints on both the number of factors and the number of levels for each factor

that can be handled. For example, Plackett–Burman (PB) designs are very efficient screening methods used to detect large main effects. Since two-factor interactions are confounded with main effects, all interactions are considered not significant. They allow to reduce drastically the number of runs required but can be applied only with 2-levels factors. Box–Behnken (BB) are instead response surface designs, used when the objective is to find an optimum yield. In these cases the model has to be able to capture a curvature to identify a maximum (or minimum) value of the response. Thus, 3 levels are strictly needed for each factor. Orthogonal Arrays are one of the most common designs: they consist of Fractional Factorials where the orthogonality between the factors is kept [26]. In this way, the effect of factors on the response can be estimated independently of each other. However, they have strict constraints on factor-level combinations which often make their application impossible [29].

A method that can be used regardless of the input parameters or the objective, is the D-Optimal criteria [26]. In addition, it can manage whatever process model, also with interaction and quadratic effects. It is not a technique that gives a predefined experimental matrix, but it is instead a methodology useful to compare the quality of different matrixes and identify the best one regardless of the design space chosen. The idea behind this methodology can be explained by analyzing the matrix form of the model:

$$\mathbf{Y} = \mathbf{X}\boldsymbol{\beta} + \boldsymbol{\epsilon} \tag{3}$$

Here, for a main-effect model with n runs and k factors, $\mathbf{Y}$ and $\boldsymbol{\epsilon}$ are vectors with n components, $\mathbf{X}$ is the model matrix of dimensions $[n\cdot(k+1)]$ and $\boldsymbol{\beta}$ is a vector with $(k+1)$ elements corresponding to the intercept β_0 and the k main effects. If also two-factor interactions are analyzed, $k(k-1)/2$ estimates are added to the model. The variance–covariance matrix of the vector of parameter estimates $\hat{\boldsymbol{\beta}}$, in a least-square analysis is equal to $\sigma^2(\mathbf{X}^T\mathbf{X})^{-1}$. The variance parameter σ^2 is an unknown constant: when planning an experiment, σ^2 is set to one and only the elements of $(\mathbf{X}^T\mathbf{X})^{-1}$ are considered. The diagonal elements of the variance–covariance matrix are the parameter estimate variances $\mathrm{var}(\hat{\beta}_i)$. The off-diagonal elements are the covariances between pairs of estimates $\mathrm{cov}(\hat{\beta}_i, \hat{\beta}_j)$ [29].

In the D-Optimal criteria, the goodness of experimental designs is quantified by means of the *D-efficiency*.

$$\text{D-efficiency} = 100 \cdot \frac{1}{n \cdot \det((\mathbf{X}^T\mathbf{X})^{-1})^{1/p}} \tag{4}$$

where n is the number of runs and p is the number of estimates. The D-efficiency increases as the parameter estimate variance decreases. Thus, the D-Optimal criterium tries to minimize the variance of the parameter estimates for whatever process model (3) and for whatever design space chosen ($\mathbf{X}$). For an orthogonal design, the variance–covariance matrix is diagonal and its determinant is equal to $1/n$ making the D-efficiency 100%. Thus, D-efficiency measures the goodness of a design with respect to a hypothetical orthogonal design, whose D-efficiency is 100% by definition. These orthogonal designs might not exist for a specific application, i.e. for a specific factor-level combination and process model chosen. The D-efficiency is not useful as an absolute measure, but it should be used relatively, to compare one design to another for the same application. This highlights again the importance of contextualization for the choice of the optimal experimental design. Depending on the specific application, efficiencies that are not near 100% might be perfectly satisfactory. When D-efficiency is 100%, then the design is balanced and orthogonal.

Table 2 summarizes the key characteristics of different DoE methods used to define experimental matrices. These characteristics include the main advantage of each method, the number of runs required, and whether constraints are present regarding the combination of factors and levels. It is clear how the D-Optimal criterium is the most flexible. However, building an experimental matrix using the D-Optimal criteria is not straightforward, unlike other methods for which predefined matrices are readily available in textbooks or online resources. This difficulty may explain why the DoE approach has never been applied to the test case described in this paper and is rarely used in other multi-phase flow applications. Although DoE methods are well-suited for complex analyses like the one involving multi phase flows, the number of factors and levels involved often excludes the use of standard methods. In light of this, the novelty of the study is further reinforced.

3. Phase 1 - Problem layout

3.1. Objectives and parameters in charge

As previously introduced, the first step for the selection of the optimal design involves the definition of the problem layout. This phase comprehends the statement of the research question that we are trying to answer and the choice of factors, levels, and response variable. For this specific application, the main objective was to assess and quantify the flow phases distribution in the channels of an evaporator header with an air–water mixture, and to explore **if and how** the combination of different design and operating variables had an effect on the distribution. For this reason, the process model was explicited via the following equation, with both main, second-order effects and two-way interaction terms:

$$y = \beta_0 + x_i\beta_i + x_i^2\beta_{ii} + x_i x_j \beta_{ij} \tag{5}$$

To properly select the response, factors, and levels involved, an in-depth examination of the physical phenomena was necessary. In literature, the goodness of phases distribution is often quantified in terms of the standard deviation of the mass flow rate [16,30], as it measures how far is the actual distribution from the ideal even one. Besides, the liquid phase flow rate is almost always used as a reference since the liquid phase is the most critical in an evaporation process. Thus, it was chosen as the response also for this specific case via the following equation:

$$y = \sqrt{\frac{1}{n-1}\sum_{i=1}^{n} |\dot{m}_{water,channel,i} - \mu|^2} \tag{6}$$

where n is the number of channels and μ is the mean water flow rate over the channels, defined as:

$$\mu = \frac{1}{n}\sum_{i=1}^{n} \dot{m}_{water,channel,i} = \frac{\dot{m}_{water,inlet}}{n} \tag{7}$$

For what concerns factors and levels, as shown in the introduction, the parameters impacting the two-phase flow distribution inside an evaporator header are numerous and of various origins. However, they can be distinguished between having a minor or a major impact. Although header-channels orientation is one of the most influential parameters, researchers often concentrate on a single configuration for ease of implementation. Even in studies where various orientations are analyzed, results usually differ across configurations due to physical deviations in the underlying phenomenon. Thus only one configuration – horizontal header with vertical downward channels – was chosen for the present test case, as the focus is on the DoE approach methodology. For a given header orientation, the parameters that most affect the phase distribution were found as the inlet tube position, channels' intrusion, and flow regime at the inlet pipe. In addition, the presence of a separated two-phase pattern at the header inlet usually worsens the distribution. Thus, the use of a splashing grid at the header inlet is one of the simplest and most effective adjustments to create a more homogeneous flow of vapor and small liquid droplets in the manifold [31]. All the cited parameters were chosen as factors for the present case study. The inlet flow pattern was represented by air and water flow rates, as it was experimentally varied by adjusting these flow rates. The ranges of air and water flow rates chosen allowed to test all the relevant flow regimes at the header inlet, from bubbly, to slug and up to annular flow. The list of selected factors and respective levels in

Table 2
Summary of main characteristics of existing DoE methods.

	Full factorial	Box–Behnken	Plackett–Burman	D-Optimal
Main advantage	Most detailed analysis, information on all interactions	Estimate interactions and quadratic effects	Evaluation of only main effects	Always applicable
Number of runs	Maximum, all combinations are tested	Medium compared to Full Factorial	Very small compared to Full Factorial	Flexible, depends on resources
Constraints on factors and levels	Yes	Yes	Yes	No

Table 3
Factors, numbers and descriptions of levels for the specific tests case.

Factor	Levels	
Inlet tube position	3	Position −1 : horizontal inlet Position 0: lateral vertical inlet Position 1: lateral central inlet
Channels intrusion	3	Intrusion −1 : 0 mm Intrusion 0: 33 mm Intrusion 1: 66 mm
Splashing grid	2	Grid −1 : grid not present Grid 1: grid present
Water flow rate	2	Water −1 : 0.18 m^3/h Water 1: 0.37 m^3/h
Air flow rate	3	Air −1 : 6 m^3/h Air 0: 18 m^3/h Air 1: 30 m^3/h

charge that define the **design space** are shown in Table 3. The right column displays, for each factor, the description of all level *labels* to which we will refer in the following part of the paper. For example, *Position −1* describes horizontal inlet, *Position 0* to lateral vertical, and so on. Additional information on the factors and respective levels is given in the description of the test section in Section 3.2.1.

In the model described by Eq. (5), with 5 factors 21 contributions are present: the intercept β_0, 5 main effects $x_i\beta_i$, 5 s order effects $x_i^2\beta_{ii}$, and 10 interaction terms $x_i x_j \beta_{ij}$. In the following section, the x_i components of Eq. (5) will be indicated as p, i, g, w, and a: they indicate the levels of position, intrusion, grid, water, and air respectively. Water and air flow rate ranges were chosen based on the availability of the facility. The values representing the different levels were set between −1 (lowest level) and 1 (highest), both for continuous factors and for discrete ones. This is a common practice in DoE applications, as it allows to scale the results equally and to compare all the effects with the same level of importance. In addition, models with interaction terms always have the main effects correlated if the factors are not scaled. This could lead to incorrect conclusions.

This ends Phase I: after defining the objectives, process model, and parameters to be analyzed, it is time to define the experimental matrix. Before passing to Phase II, a description of the experimental layout and of all the different levels selected is shown in the next subsection.

3.2. Experimental set-up

3.2.1. Test section

A detailed view of the test section is shown in Fig. 2(a). It consists of a horizontal header and eight parallel downward channels, modeling a simplified version of an evaporator. The manifold is made of aluminum, with a rectangular section of (186 x 130) mm, 560 mm long. The lateral walls of the header are made of plexiglass to allow flow visualization.

The inlet feeding pipe is 1 m long with a diameter (D) of 23 mm. Being almost 50D long, it ensures a fully developed flow at the header inlet. It is made of stainless steel except for 65 mm before the manifold, where it is screwed onto a plexiglass block. This block has two polished lateral faces, enabling visualization of the flow regimes at the header inlet. Between this block and the header entrance, the 3D printed resin splashing grid can be inserted. It consists of homogeneously distributed small holes on a slightly spherical surface. The holes have a diameter of 0.5 mm and are distanced 1.5 mm between each other. A scheme of the grid is shown in Fig. 3.

Three inlet pipe positions have been chosen: they are specified in Fig. 2(a); *Position −1* is referred to the horizontal, *Position 0* to the lateral vertical and *Position 1* to the central vertical inlet. In this way, all the inlet pipe position configurations were incorporated into the experimental activity, including both coaxial and parallel orientations relative to the header. For the parallel configuration, both symmetric and asymmetric positions with respect to the header center were considered.

Eight tubes of 10 mm diameter made in stainless steel are connected to the manifold. Venturi flowmeters are installed in each channel to obtain the total mass flow rate, as well as pressure sensors to monitor the static pressure. The differential pressure across the flowmeters is measured by means of a pressure membrane sensor (Validyne DP15 with a 350 mbar range). All the Valydines are placed at the same height with respect to the test section, and the pressure lines connecting them to the ports are all of the same lengths, to avoid differences between channels. The static pressure sensor is positioned at 70 mm from the top of the tube. Upstream and downstream pipes of 520 and 170 mm lengths are available respectively before and after the Venturi. More details about the Venturi design and calibration are given in [32].

Each channel has three flanges for the installation of stainless steel spacers, which served to test the various intrusion levels. This allows to study easily several intrusion depths, going from no intrusion (*Intrusion −1*), to an intrusion of the channels inside the header of $\frac{1}{4}$ (*Intrusion 0*), and $\frac{1}{2}$ (*Intrusion 1*) of the height of 130 mm, covering all the intrusion cases mainly reported in literature, ranging from zero up to half the height of the header. Finally, the flow passing through the 8 tubes is collected into a 200 mm circular test section 590 mm long.

3.2.2. Experimental loop

A schematic view of the experimental setup is shown in Fig. 4. Water flow is pumped from an open reservoir by a centrifugal pump (Wilo) inside the circuit. After the pump, a bypass loop allows the water to be re-injected into the reservoir. The water flow rate can be changed by adjusting the valve $V1$ of the bypass loop. The air flow is taken from the 40 bar compressed air line. A pressure regulator sets the air pressure upstream of the circuit to 1.5 bar: its flow rate can then be varied by adjusting valve $V2$ of Fig. 4. The water flow rate is measured with an electromagnetic flowmeter (Fuji ElectricModMAG®M1000), while the air flow rate is measured thanks to a thermal mass flow sensor (CS Instruments VA 500). Water and air flow rates are then mixed and able to reach the inlet feeding pipe of the test section. The fluid total pressure was monitored inside the water and air inlet pipes, inside the header, and inside each of the eight channels using flush-mounted absolute pressure sensors (YA1014ABS/10V244 from C2AI). The fluid total temperature was monitored at the water and air inlets using type K thermocouples.

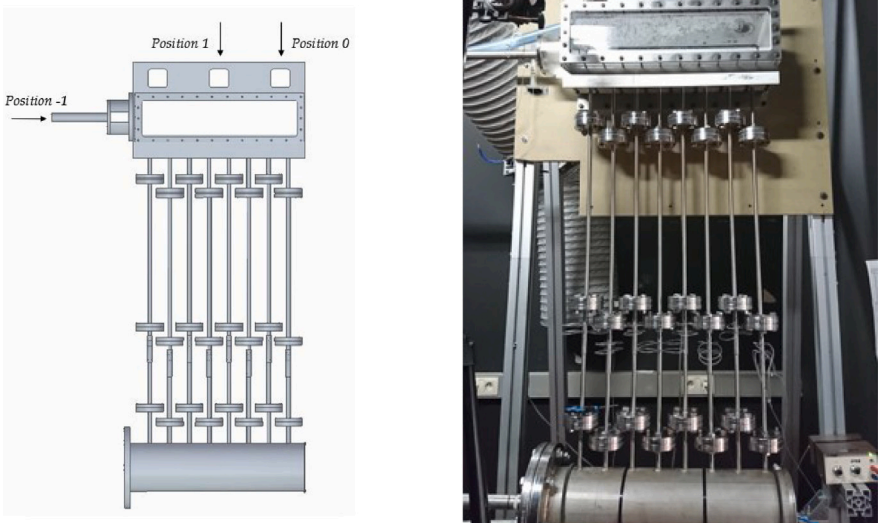

(a) *Scheme* (b) *Picture*

Fig. 2. Schematic and picture of the header and channels.

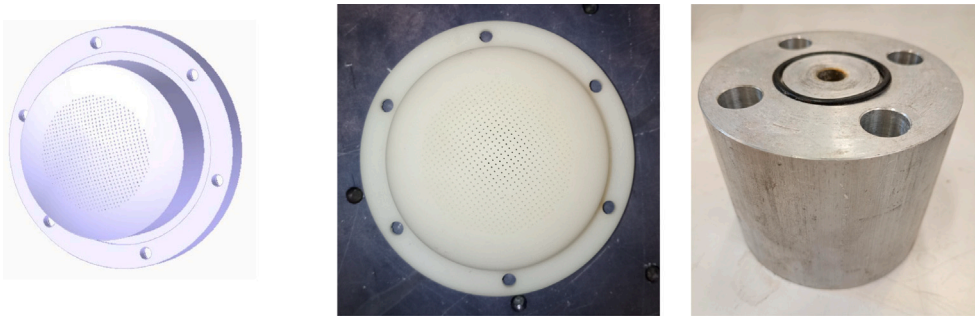

(a) (b) (c)

Fig. 3. Schematic (left) and picture (center) of the splashing grid; picture of the spacer for increasing channels intrusion (right).

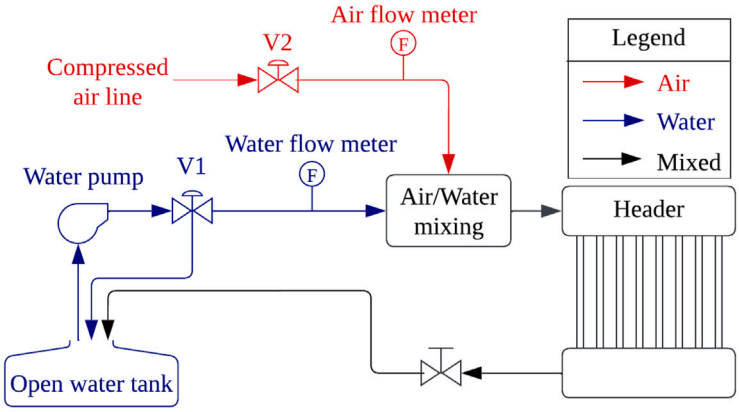

Fig. 4. Schematic view of the experimental facility.

3.2.3. Data collection

A challenge that arises when testing gas-liquid flows lies in wall pressure measurements. Indeed, they must be made with minimum flow disturbance and with the guarantee of the presence of a single phase in all pressure lines. Purging is a well-known technique to ensure that pressure lines are always filled with water. During preliminary tests, measurements were taken under the same flow conditions, with and without purging. From these measurements, it was confirmed that a high presence of bubbles in pressure lines introduced large distortions and non-repeatability of the signal. Thereby, the first step in the experimental procedure consisted in filling the channels with water and purging all the Valydine's pressure lines from air bubbles. Still, as soon as the air started flowing through the circuit, small air bubbles were eventually going in the lines, but not significantly affecting the signal. Thus, purging was repeated whenever a considerable amount of air bubbles was present in the pipes. In addition, for each different testing day, an *offset* measurement was recorded for each Valydine. This consisted in the differential pressure acquired with the circuit still, and the pressure lines filled with water. Every measurement taken during each testing day was then subtracted by the respective *offset* value. This ensured no discrepancies between testing days (because of different atmospheric conditions) nor between channels (because of differences between pressure lines).

At the start of each test, the air and water flow rates were set by adjusting valves V2 and V1 of Fig. 4 respectively. Once stable conditions were reached, the differential pressure across Venturi flowmeters was recorded through Valydine DP15 sensor with 350 mbar range. To visualize the two-phase flow distribution in the header, a DANTEC high-speed camera was used. This recording was also compared to the distribution profile obtained from the determination of the flow rate and quality using the Venturi solely. All the instrumentation, except for the high-speed camera, was connected to a National Instruments data acquisition system (NI-DAQ). The signals were acquired at a frequency of 200 Hz over a duration of 90 s.

The individual air and water flow rates in each of the eight channels, $\dot{m}_{air,channel_i}$ and $\dot{m}_{water,channel_i}$, as well as the quality, were calculated from the Venturi pressure drop $\Delta P_{venturi,TP}$ measurement and a robust calibration dataset obtained prior to the experimental campaign. For each channel, the uncertainty associated with the pressure measurements was computed from the Valydine calibrations, assuming a t-student distribution for the fitting error and considering a 95% confidence interval. The computed uncertainties are all comprised between ±0.178 and ±1.299 mbar. For additional information on the computations of air and water flow rates, the readers are kindly referred to the article of Lecardonnel et al. [32] in which the calculation methodology is wholly described. The authors propose a new iterative methodology to predict the vapor and liquid phase flow rates in each channel, based on Venturi pressure drops measurement solely. In the present work, the methodology was adapted to atmospheric conditions. Following the work of [32], the accuracy of the individual air flow rate measurement is expected to be ± 20% of error at maximum on average, while the accuracy for the water flow rate is expected to be below ± 10% in average. The detailed explanation of the uncertainties quantification can be found in [32].

4. Phase 2 - Definition of experimental matrix

As previously stated, Phase 2 is the heart of the process: it involves the choice of the DoE technique to be applied for the specific application. For the present case study, the combination of factors and levels in charge made it impossible to choose an already existing experimental design. In fact, the problem involved 3 factors with 3 levels and 2 factors with 2 levels (Table 3). Despite the abundance of methods available, it was necessary to find a non-conventional way to define the experimental matrix.

Table 4
Efficiencies with varying number of runs.

Runs	54	72	108
Orthogonality	99.9	100	100
Center Balance	100	100	100
Level Balance	100	100	100
Two-level Balance	99.6	100	100
Two-level Missing	100	100	100
D1-Efficiency	81.6	81.7	81.7
D2-Efficiency	67.3	67.3	68.4

The experimental matrix was created by means of the Python package DoEgen [33], which combines optimality criteria and finds the best matrix for a given set of parameters in input. For a given design space, the program creates various experimental matrixes with an increasing number of runs. For each case, it then computes 7 *efficiencies* to evaluate the best configuration; they quantify (1) how close each matrix is to an orthogonal one (Orthogonality), (2) how well it is centered between factors (Center balance), (3) levels (Level balance), (4) levels in pairs of factors (Two-level balance) and (5) factor-level pair combination (Two-level missing). In addition, it gives the D-efficiency for a model with main and two-way interaction terms ((6) D-Efficiency) and with also quadratic terms ((7) D1-efficiency). As a result, the program gives as output different experimental designs with an increasing number of runs, and it automatically suggests a minimum, optimal, and best design from the ones created based on the efficiencies computed. The experimentalist, given the amount of time and resources that he can spend on the specific application, i.e. the maximum allowable number of runs, can choose the optimal test planning.

For the present test case, a Full Factorial would have required 108 number of runs. The efficiencies were computed with designed matrixes from 24 to 108 runs, and are shown in Fig. 5. Although even 54 tests gave high coefficients, the best design required 72 runs and was therefore selected as it fell within the allowable test number. Indeed, with this design, the efficiencies are slightly higher (Table 4). In addition, all the geometric layout combinations are tested with 72 runs. The number of runs was thus decreased by 33% globally.

5. Phase 3 - Results

The third and last part of the DoE methodology involves the test execution and the analysis of results, which are shown in this section. Firstly, the randomness assumption is described and verified for the present test case. It is part of a preliminary analysis that should always be performed when analyzing experimental results. Then, the important sources of variability are examined, and the effect of each factor and their combination is analyzed and quantified. Lastly, the best configuration is confirmed, and a first attempt at process modeling is performed.

5.1. Preliminary analysis - Randomness assumption

Randomization is a fundamental technique of experimental design. Lack of randomness leaves the experimental procedure open to both systematic and experimenter bias [28]. It can reveal, for example, a time-effect of the experimentation. The first step that was done before starting analyzing DoE results, was thus to check whether there were any non-random patterns in the output data. In that case, the validity of the scientific conclusions would not be valid. Non-random patterns can be detected by analyzing the autocorrelation of the output data set: it is defined as the correlation between y_i and y_{i-k}, where y_i is the response of the ith run, and k is an integer that defines the lag. For a random data set, autocorrelation is near zero for all lags. If it is not, one or more of the values will be significantly non-zero. The trend obtained in the present case study is shown in Fig. 6. The horizontal lines displayed in

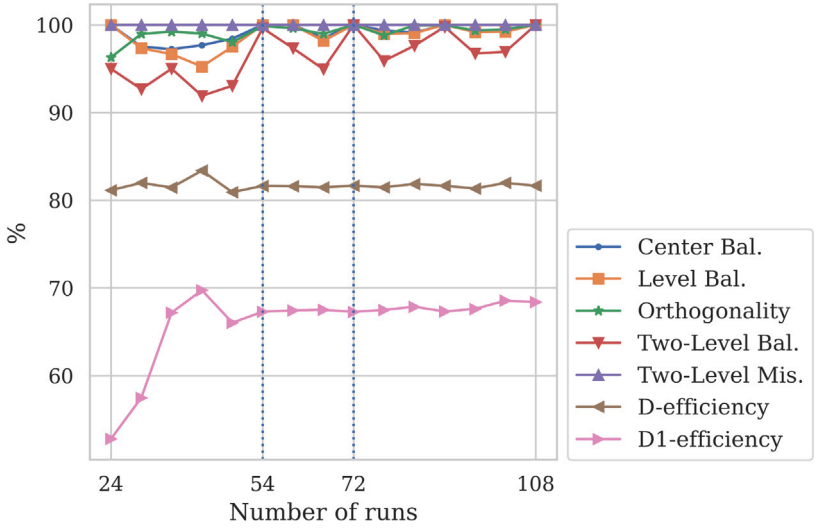

Fig. 5. Matrix *efficiencies* with increasing number of runs.

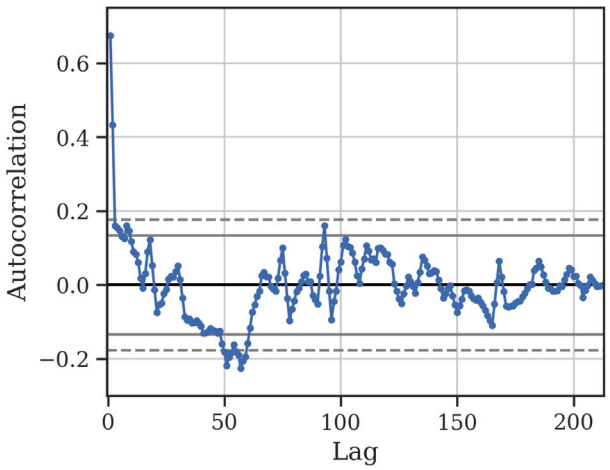

Fig. 6. Autocorrelation as function of lag with all tests.

the plot correspond to 95% (continuous line) and 99% (dashed line) confidence bands, whose values were obtained via the formula:

$$\pm \frac{z_{1-\alpha/2}}{\sqrt{N}} \tag{8}$$

Here z is the cumulative distribution function, α is the significance level and N the number of runs.

The lag 1 autocorrelation has a significantly high value. This happens because, for each run given by the experimental matrix, 3 samples were acquired for repeatability. Indeed, looking at the lag 3 autocorrelation, it is widely inside both the 95% ($[-0.134; 0.134]$) and 99% ($[-0.176; 0.176]$) confidence band. The lag 3 autocorrelation is not statistically significant: thus, there is no evidence of non-randomness, and the following statistical analysis can be trusted.

5.2. Main and interaction effects

The investigation of main effects is one of the most common outputs from a DoE analysis. Using this tool, a ranked order of the most influential factors can be obtained. The so-called "DoE Mean plot" (Fig. 7) is used for this purpose. It indicates the mean of the response variable (y-axis) for each level of the factors (x-axis). The levels are displayed, for each factor, with their corresponding number. Looking at the variability of the response for different levels of each factor, we can assess the ranked list of most affecting parameters. Air flow rate has significantly the highest effect, followed by channels intrusion and inlet pipe position. Instead, the presence of the splashing grid and the water flow rate do not seem to have any effect on the output. From the DoE Mean Plot, we can have an indication of the best combination of parameters. As previously stated, the response is the standard deviation of water flow rate across all channels. Thus, the optimal configuration is the setting that minimizes the response: it is expected with horizontal inlet (*Position −1*), with highest channel intrusion (*Intrusion 1*), and highest air (*Air 1*) flow rate.

These would be the conclusions from an exploratory analysis when the experimentalist is interested in having a first indication of the factors that may or may not have an impact on the response. When a high number of parameters is involved, looking at only main effects can reduce strongly the number of required runs. This type of plot is what would come out from the analysis, and the experimentalist could then focus on the variables of interest, investigating more in detail the effect of the most important factors. However, looking at only main effects could hide some important dependencies. If we had based our result analysis only on main effects ($x_i\beta_i$), we would have concluded that the presence of the grid and the water flow rate are not influencing the results. For a clear understanding of the phenomena also interactions ($x_i x_j \beta_{ij}$) need to be examined.

From a graphical point of view, the two-way interaction effects can be analyzed by means of the DoE Mean Interaction Plot: it is equivalent to the DoE Mean Plot, but it considers the interaction between factors. In Fig. 8, the mean response is shown on the y-axis as a function of all the two-way parameters $x_i x_j$. Each curve is relative to one of the interaction terms labeled on the x-axis. For each curve, the left point displays the mean response with $x_i \cdot x_j$, i.e. with the product of the level values, equal to −1. Towards right, the middle point displays $x_i \cdot x_j$ equal to 0, and the right point displays $x_i \cdot x_j$ equal to 1. For each curve, higher variation between the 3 combinations indicates a higher impact on the output. The factors that have the highest combined effect on the response are inlet pipe position and splashing grid (PG), followed by channel intrusion and water flow rate (IW) and presence of the grid and air flow rate (GA). Then, a medium effect is given by all the other interaction terms combined with channels intrusion (PI), (IG) and (IA). Lastly, the remaining terms have the lowest impact.

From this analysis, we can already conclude that looking at only main effect is not sufficient for a clear understanding of the phenomena. From Fig. 7, water flow rate seemed a not influential factor; however,

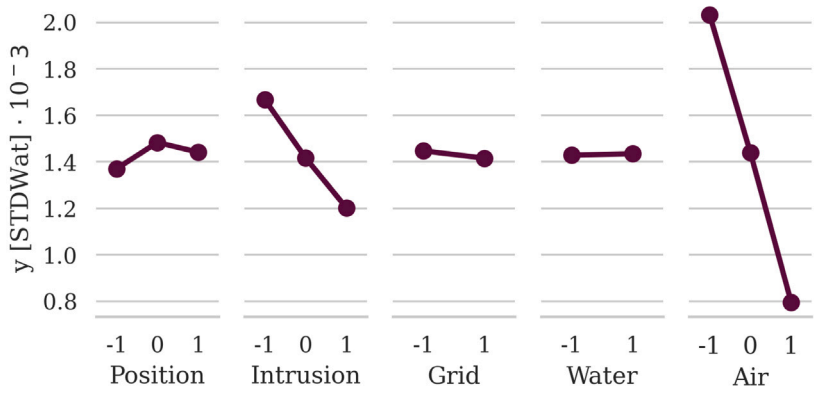

Fig. 7. DoE Mean plot.

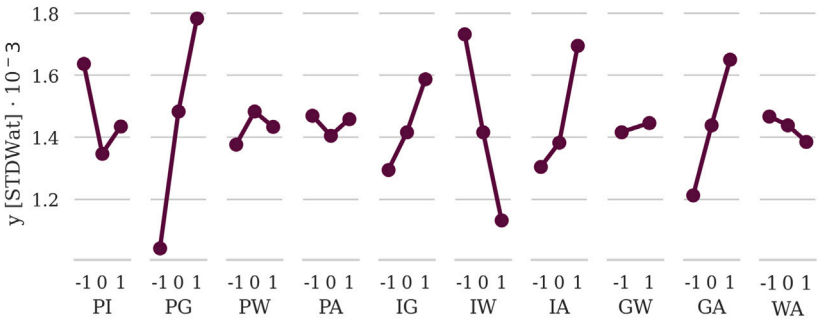

Fig. 8. DoE Mean Interaction Plot.

when combined with channel intrusion, it is one of the strongest two-way interactions.

Going deeper into the analysis, results can be analyzed for each interaction term through box plots: these are graphical tools used to display the distribution of a data set by means of their quartiles. As shown for instance in Fig. 9(c), a box plot is displayed as a rectangular shape: the range within the rectangle represents 50% of the data set, between the 25th (lower horizontal line of the rectangle) and the 75th (higher horizontal line of the rectangle) percentile. The mid-line inside the rectangle represents the median, while the horizontal lines outside the rectangle represent the maximum and minimum values. For this test case, results are presented through box plots showing 2 factors at a time, a *Primary Factor* and a *Secondary Factor*. For the so-called *Primary Factor*, different factor levels are displayed on the x-axis; for the *Secondary Factor*, different factor levels are displayed in consecutive rectangles of different colors. For example, looking at Fig. 9(c), Position is the *Primary Factor* and Grid is the *Secondary* one. Position levels are displayed on the x-axis, with −1 on the left, 0 in the center, and 1 on the right. Grid levels are represented with different colors – blue for −1 and orange for 1 – and on consecutive boxes. In addition, in the plots shown herein, each observation is shown as a point. All the relevant box plots are shown and commented in the following subsections, together with the two-way interaction curves.

5.2.1. Position

The mean interaction between Position levels and all other factors is shown in Fig. 9(a); the highest effect is given by the term *PG*, which is thus investigated in the box plot in Fig. 9(c). Without the Grid (*Grid* = −1, blue) the response becomes lower passing from the horizontal inlet (*Position* = −1, left) to the vertical ones (*Position* = 0 and 1, center and right). Instead, the presence of the Grid (*Grid* = 1, orange) gives a better, i.e. lower, response with horizontal inlet (*Position* = −1, left). This is a great outcome since the grid was firstly designed by Ahmad et al. [31] for horizontal pipes, and expected to perform better for this pipe orientation than for a vertical one.

The combination of Position and Intrusion seems to be affecting the output from Fig. 9(a). From the box plots in Fig. 9(b), it is clear that the highest Intrusion level (green) has a positive effect for Position = −1 and Position = 0. No direct conclusion can be drawn for Position = 1.

For what concerns Position and Air levels, even though their interaction is not significant, the box plot in Fig. 9(d) confirms that for all Position levels, increasing the air flow creates a clear improvement in the response; the highest Air level (green) has, for all cases, lower median response and variability. The conclusion regarding the combined effect of airflow and inlet tube position is logical. Increasing the airflow increases the velocity of the two-phase flow. By increasing its inertial forces for a vertical inlet, the annular flow is projected against the opposite wall at the bottom of the header. This creates a large liquid wave that can feed channels further away from the inlet. This is in line with was has been reported also by Fei et al. [17] and Ahmad et al. [31]. With a horizontal inlet, as the air flow rate increases, so does the power of the inlet jet created, allowing the two-phase flow to reach channels at the rear part of the header. The phenomenon is similar for the presence of the grid, which also accelerates the flow and distributes the two-phase flow throughout the header in the form of a multitude of fine jets. For this reason, the presence of the grid and a horizontal inlet position improve the distribution. On the other hand, with a vertical inlet and the grid, while the presence of the latter helps to accelerate the flow, the fine jets created tend to overfeed the channels opposite the inlet and do not create a wave as the annular jet did.

5.2.2. Intrusion

The mean interaction between Intrusion levels and all other factors is shown in Fig. 10(a). All factors seem to interact with Intrusion levels, even if a clear trend is missing for Position (IP).

The interaction between Intrusion and Grid is shown in Fig. 10(b). Without the presence of the Grid (*Grid* = −1, blue) the response gets better with increasing Intrusion: indeed, the blue rectangles in

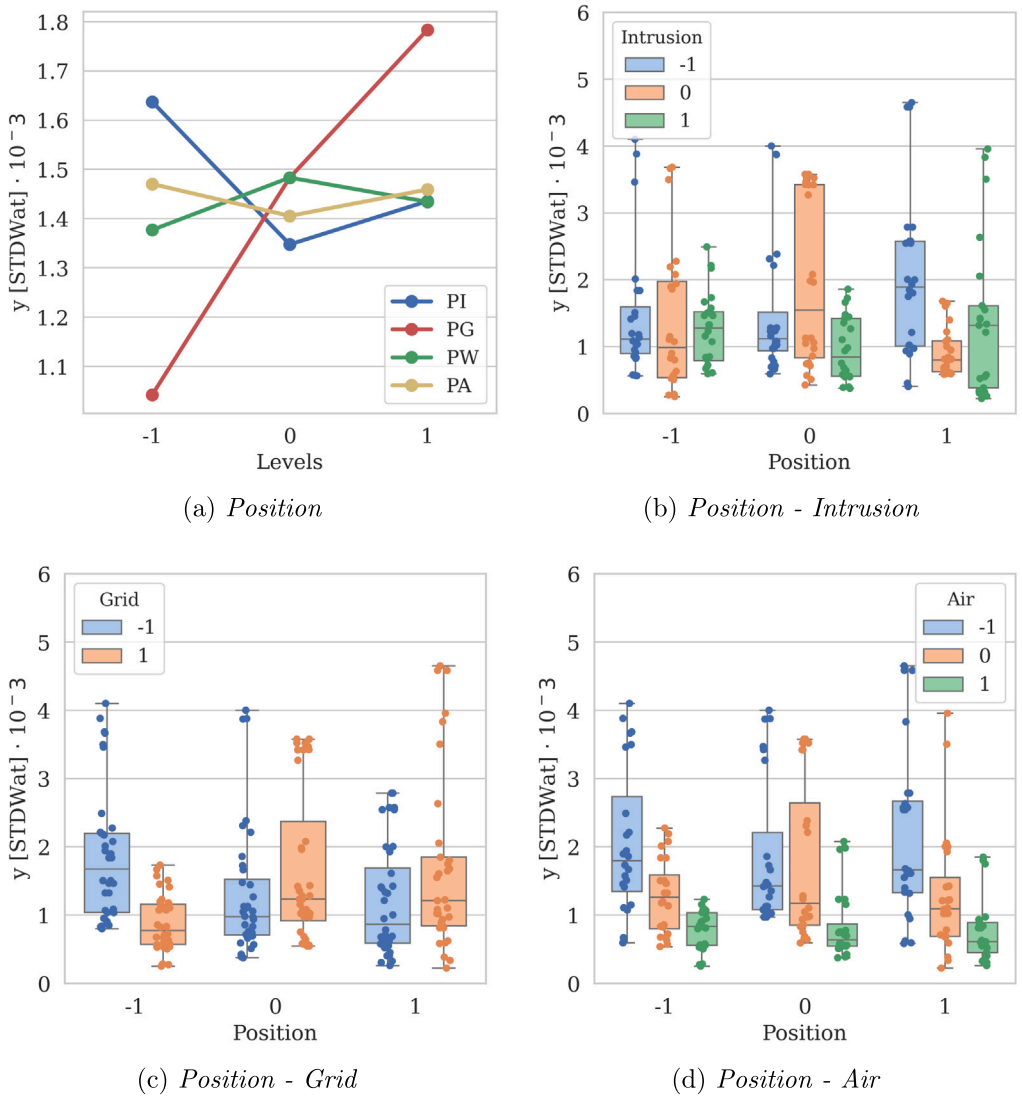

(a) *Position* (b) *Position - Intrusion*

(c) *Position - Grid* (d) *Position - Air*

Fig. 9. Position levels.

Fig. 10(b), are gradually smaller and with lower variation going from the left to the right of the plot. Indeed, as the intrusion increases, a water pond is created at the bottom of the header when the grid is missing. The higher the intrusion, the deeper the pond, as also reported by Dario et al. [4], and so the better the distribution among the channels due to the better propagation of the waves created at its surface.

With the Grid instead (*Grid* = 1, orange) the trend is more blurry: apart from some outliers with the lowest Intrusion levels, the orange lines (*Grid* = 1) cover higher ranges going from the left to the right of the plot, indicating a worsening in the output. However, the median value is similar for all intrusion levels: with the presence of the grid, the variation of channel intrusion does not have an absolute effect on minimizing the response, but lower intrusion reduces the variability of data. This mixed trend indicates that this combined effect also depends on the interaction with a third or even fourth parameter, for instance the inlet tube position or the air mass flow rate.

For what concerns Intrusion and Water (Fig. 10(c)), a strong effect is experienced. Looking at the blue rectangles, which are referred to *Water* = −1, the response gives smaller ranges as the Intrusion level gets smaller. On the contrary, the highest Water level (*Water* = 1, orange) gives the exact opposite results: the rectangles become smaller and lower with increasing Intrusion levels. The interaction between *Intrusion* and *Water* is thus significant for the analysis of results.

Regarding Intrusion and Air (Fig. 10(d)) it is clear that higher Air (green) has a positive effect on the response. From this plot we can also see that with the highest Intrusion (*Intrusion* = 1, on the right) the rectangular are small for all Air levels: this indicates the ability of the highest Intrusion level to give responses with lower variability, as data in the 25–75 percentiles range are in a narrower region. Similarly to what has been explained in Section 5.2.1, the increase of the air flow rate causes an augmentation of the inertial forces. This improves, whatever the intrusion depths are, the dispersion of the two-phase flow inside the header and thus the flow feeding among the channels. This is especially true at higher intrusion, since it generates waves of stronger amplitude at the surface of the water pond created at the bottom of the header, as the air mass flow increases. This is in line with the main conclusions from the literature. Especially for horizontal headers, the tube intrusion is mentioned as one possible way to improve the two-phase flow distribution [5,34]. Wijayanta et al. [35] studied for instance the impact of various patterns of tube intrusion on a flow of R134a inside a horizontal header connected to vertical downward channels. For every intrusion pattern, the results were still found to be better than the flush-mounted reference.

5.2.3. Grid

The interaction between Grid levels and all the other factors is shown in Fig. 11(a). The higher combined effects are experienced with

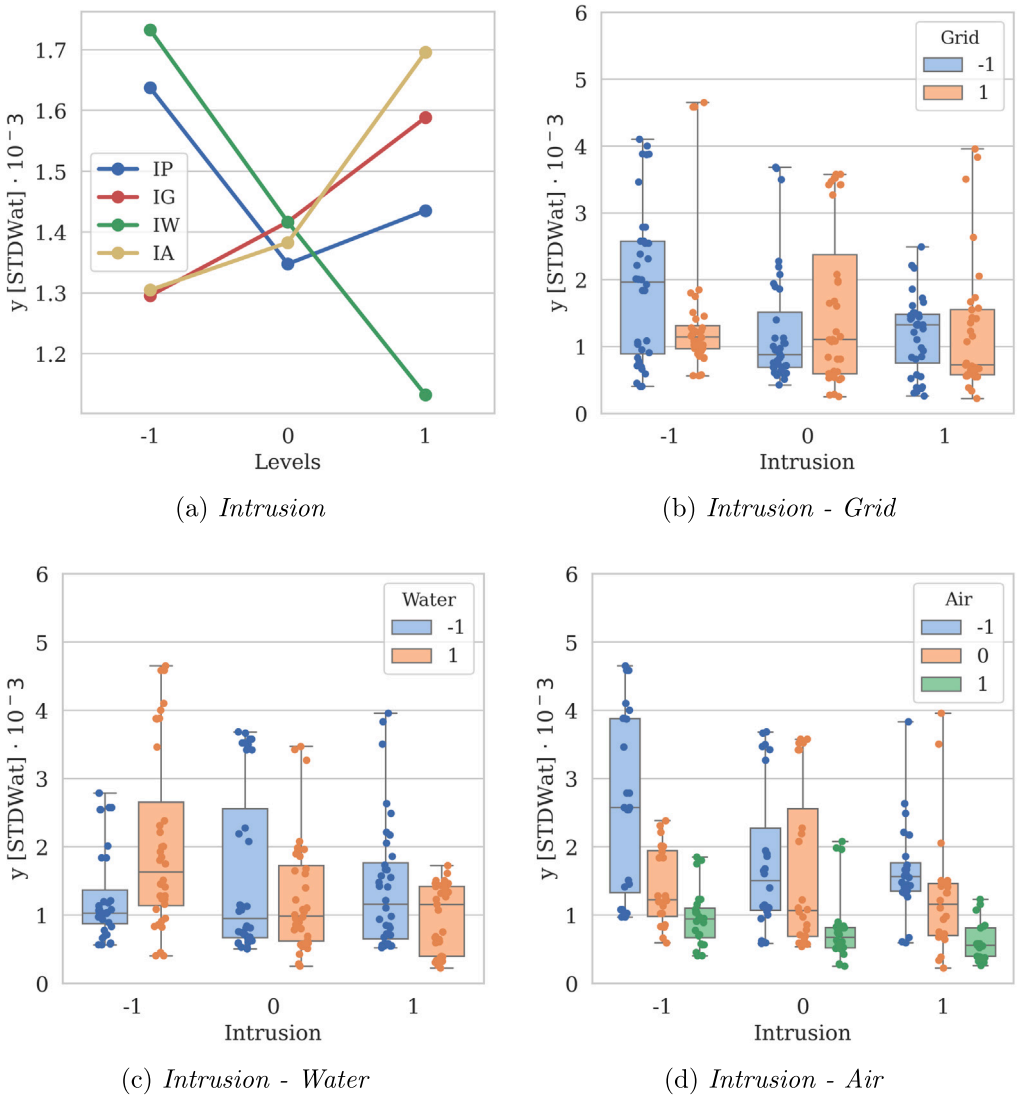

(a) *Intrusion* (b) *Intrusion - Grid*

(c) *Intrusion - Water* (d) *Intrusion - Air*

Fig. 10. Intrusion levels.

Position and Intrusion, which have already been analyzed in Figs. 9(c) and 10(b) respectively. The combined effect between Grid and Air is the following in the order of significance, and it is reported in Fig. 11(b). It again confirms that the highest Air level always gives the best response. In addition, we can see that without the presence of the grid (*Grid* = *−1*, left), results show less variability.

5.2.4. Water & Air

Fig. 12(a) shows the interaction between Water levels and all other factors. The highest effect is experienced in the combination of Water and Intrusion levels, which was already shown in Fig. 10(c). Other factors do not have a strong impact. In addition, the combined effect of Water and Air (Fig. 12(b)), again confirms the improvement given by the highest Air levels.

5.2.5. Air

Fig. 13 shows the combined effect of Air levels with all other factors. All the relevant cases have already been commented in the previous box plots. The higher combined effect is given by Intrusion (Fig. 10(d)) and Grid (Fig. 11(b)). In all cases, the highest Air level always gave the best results.

5.3. Best layout

From the DoE Mean Plot (Fig. 7), we were expecting the optimal combination of parameters with the highest intrusion (*Intrusion = 1*), horizontal inlet position (*Position = −1*) and highest air flow rate (*Air = 1*). Grid and Water levels were not apparently affecting the mean output. However, the previous discussion revealed a deeper insight into the dependency of the response on all factors. Looking at the combined effect of variables, 2 equally optimal configurations can be found:

1. With the splashing grid (*Grid = 1*), the best geometrical configuration occurs with horizontal inlet position (*Position = −1*, Fig. 9(c)) and lowest intrusion level (*Intrusion = −1*, Fig. 10(b)). The best flow rates for this configuration are the lowest for the water (*Water = −1*, Fig. 10(c)) and the highest for the air (*Air = 1*). The water level was identified thanks to the Intrusion-Water interaction. This is a very appreciable result, as the aim of the grid was to improve the distribution in the case of a horizontal inlet position, by breaking the two-phase flow structure of the input flow. Indeed, this inlet pipe orientation is often cited in the literature [4,17,31] as leading to poor distributions, with the liquid phase feeding only the channels near the inlet. The aim of the grid was therefore to allow the liquid phase to feed the channels located further away, and this is the case.

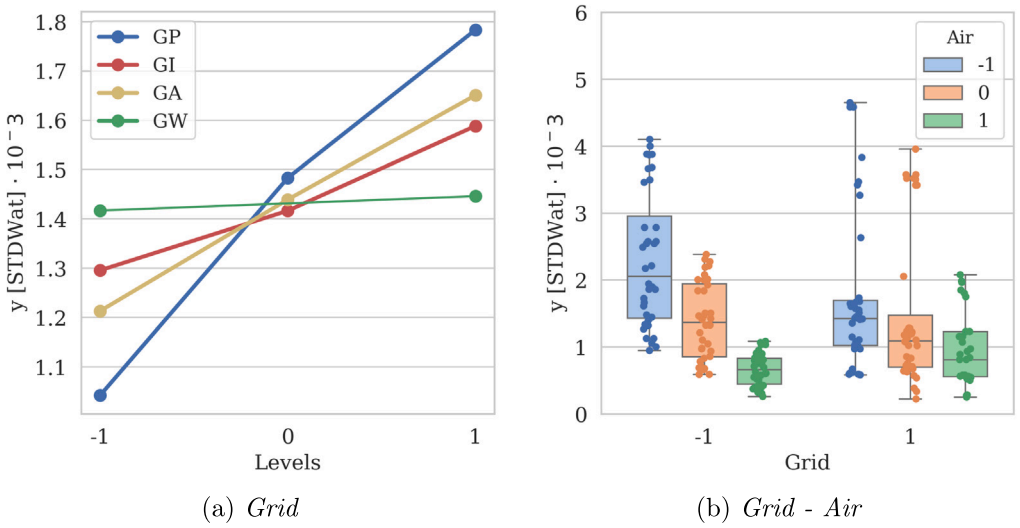

(a) *Grid* (b) *Grid - Air*

Fig. 11. Grid levels.

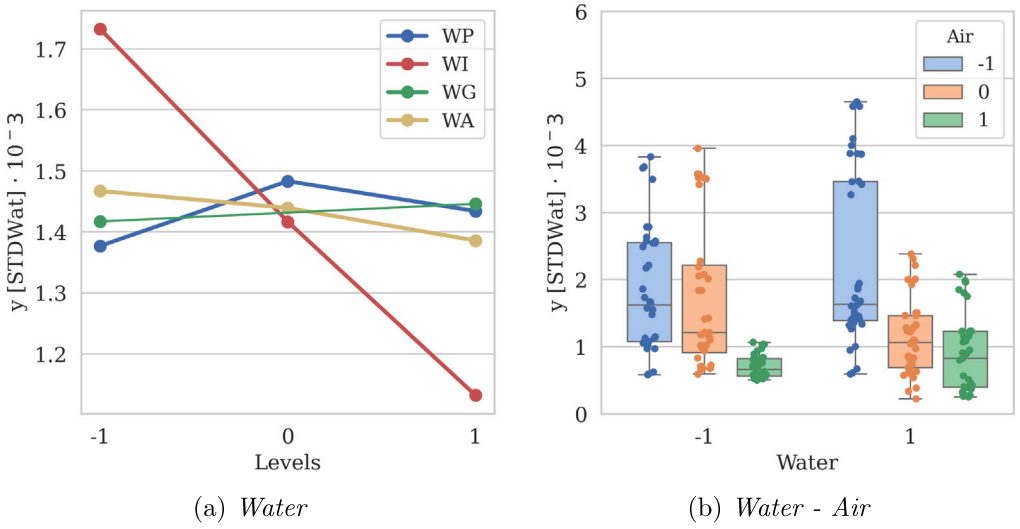

(a) *Water* (b) *Water - Air*

Fig. 12. Water levels.

2. Without the grid (*Grid* = −1), the best geometrical configuration occurs with vertical central inlet position (*Position* = 1, Fig. 9(c)), highest intrusion level (*Intrusion* = 1, Fig. 10(b)) and highest air level (*Air* = 1). Even though the combined effect of Grid and Water is not significant, the best Water level for this geometrical configuration is the highest (*Water* = 1, Fig. 10(c)), defined thanks to the Intrusion-Water interaction. This finding is also a very interesting result, as this combination of parameters was never tested in the literature and never identified as leading to a very liquid distribution. A feeding tube position perpendicular to the header but parallel to the channels was however already reported in the literature as leading to better liquid distribution than a coaxial one [36].

The factor levels of the optimal combinations are summarized in Table 5 and compared with the expected best layout from the DoE Mean plot. These results confirm the fact that looking at only the main effects and thus performing a "One-Factor-At-A-Time" campaign, can hide some interesting and significant effects on the results. A visual representation of the comparison between best and worst configurations is shown in Fig. 14 through the water flow rate distribution across the eight channels. The worst configurations have been defined with the same approach used for the bests, i.e. by looking at both Mean and Interaction plots. This result is a proof of the methodology's validity:

1. By analyzing the interactions between factors, the optimal layout identified via interaction analysis (red line) is indeed the best one, with an almost constant water flow rate in all eight channels.
2. With only main effect analysis (green line), an indication of a good layout can be obtained but it deviates from the best one. The interaction between factors is thus significant for our test case and it needs to be taken into account.
3. The worst configurations identified via main effect (blue line) and interaction analysis (orange line) are indeed giving an uneven distribution of water flow rate in the channels.

5.4. Process modeling

The concluding part of a DoE analysis can involve the development of a mathematical model for the description and, if possible, prediction of the response. The accuracy and validity of the model need to be carefully quantified, in order to define the range of applicability of the model itself. This approach is explored in this section.

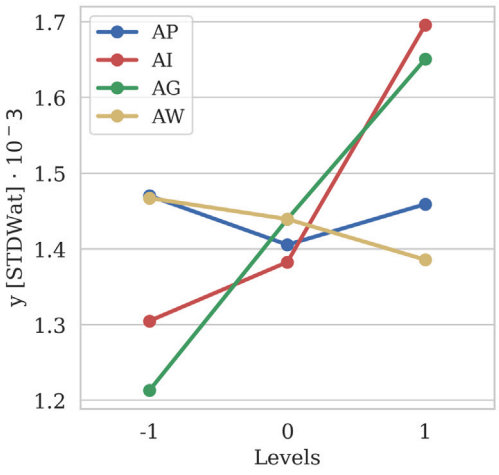

Fig. 13. Air levels.

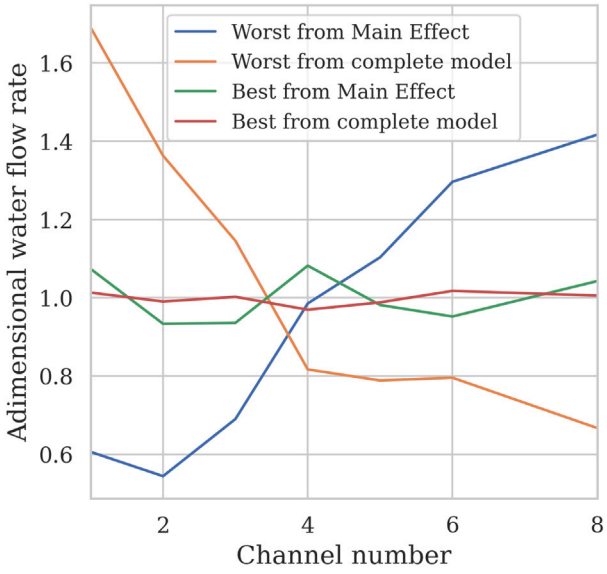

Fig. 14. Comparison between best and worst distributions.

Table 5
Best combination of parameter: looking at only main effects, or considering also interactions.

	P	I	G	A	W
Only main effects	−1	1	//	1	//
With interactions	1 −1	1 −1	−1 1	1 1	1 −1

As stated in Section 3, by taking into account all main, two-way interaction and second order terms, the relation reads:

$$y = \beta_0 + x_i\beta_i + x_i^2\beta_{ii} + x_i x_j \beta_{ij} \tag{9}$$

With 5 factors, 21 contributions are present: the intercept β_0, 5 main effects $x_i\beta_i$, 5 s order effects $x_i^2\beta_{ii}$ and 10 interaction terms $x_i x_j \beta_{ij}$. If the accuracy is not optimal, we can still use the coefficient estimates β as a quantification of the order of importance of each term, which was graphically seen in the DoE Mean plot and DoE Interaction plot. Having scaled the factor levels between −1 and 1, the magnitude of the coefficients indicates the magnitude of the consequential effect on the response. If the accuracy of the model is proven, it can also be used with confidence to predict the response.

Regardless of how many factors there are, and regardless of how complicated the model is, by looking at the behavior of its residuals, the experimentalist can verify the validity of the model itself. In particular, residuals should be random, following a normal distribution, with fixed location and fixed variation. If these assumptions are not verified, the model validity is doubtful: significant terms could be missing, or a general regression model describing the phenomena could not be appropriate for the physics beyond it. A useful tool that can be used to assess whether the validity of the modeling is acceptable, is to take a look at the so-called "4-plot". The 4-plot is a set of 4 specific graphical techniques used to test the assumptions that underlie most measurement processes [26]. By looking at the graphs shown in Fig. 15, all the hypotheses can be confirmed. The run sequence plot (on the top left) displays the residuals (y-axis) in all the runs (x-axis). The trend is (1) flat and (2) the vertical spread is approximately the same over the whole x-axis: it indicates that both fixed location (1) and variation (2) assumptions hold. The lag 3 plot (top right) shows the residuals of the ith run versus the residuals of the (i-3)th run. If the residuals are random data (randomness assumption) the experimentalist should not be able to recognize a structure in the lag plot. Equivalently to the autocorrelation plot, it can be used to verify the randomness assumption, which is confirmed. For instance, Fig. 16 shows the lag 1 plot, where a clear line can be identified: since each run was repeated 3 equivalent times, the lag 1 plot shows a clear correspondence between data. This confirms what we saw in the autocorrelation plot, where the first value was way out of the confidence interval (Fig. 6). The histogram (bottom left) and the normal probability plot (bottom right) are used to check whether the residuals follow a normal distribution. If so, the histogram should be symmetric and the normal probability plot should follow an approximate straight line. This latter shows the ordered residuals computed on the y-axis, versus the z-value from the standard normal distribution.

In our specific case, data follows approximately a normal distribution and significant outliers do not appear in the tails: it seems reasonable to assume that the coefficient estimates can be compared and the order of importance of all the contributors drawn. They are reported in Table 6 in order of importance. The second order terms are some of the less significant; a model with only main and two-way interaction terms could be an alternative with similar accuracy but smaller complexity. It would be described by this equation, decreasing the number of coefficients from 21 to 16:

$$y = \beta_0 + x_i\beta_i + x_i x_j \beta_{ij} \tag{10}$$

To be confident in the model validity for future predictions of the response, the model accuracy needs to be verified since the distribution of residuals is not perfectly symmetric. By looking at the R^2 value of the regression we can quantify the accuracy and compare different models. In our test case, R^2 value is similar for both the models developed: it is 0.5109 for the model with all second order terms (Eq. (9)) and 0.5107 for the simpler one (Eq. (10)). We can thus conclude that, for our application, a model with all second order terms does not give additional information; for the remaining part of the article, the main and two-way interaction model is considered. For brevity, the relative 4-plot is not shown here as it is almost specular to the one reported in Fig. 15.

However, the R^2 value of the regression is too low for the model to be correctly used as a predictor. Indeed, multi-phase flow increases exponentially the complexity of the process, making it difficult to obtain a universal equation capable of predicting the performances. To increase the accuracy, the authors tried a different approach, described herein. Given the significant interaction effects between factors, the dataset and thus, the models, were split into two sub-groups. In this way, instead of trying to obtain a general descriptive equation, we can narrow the field of study and search for 2 different models, each

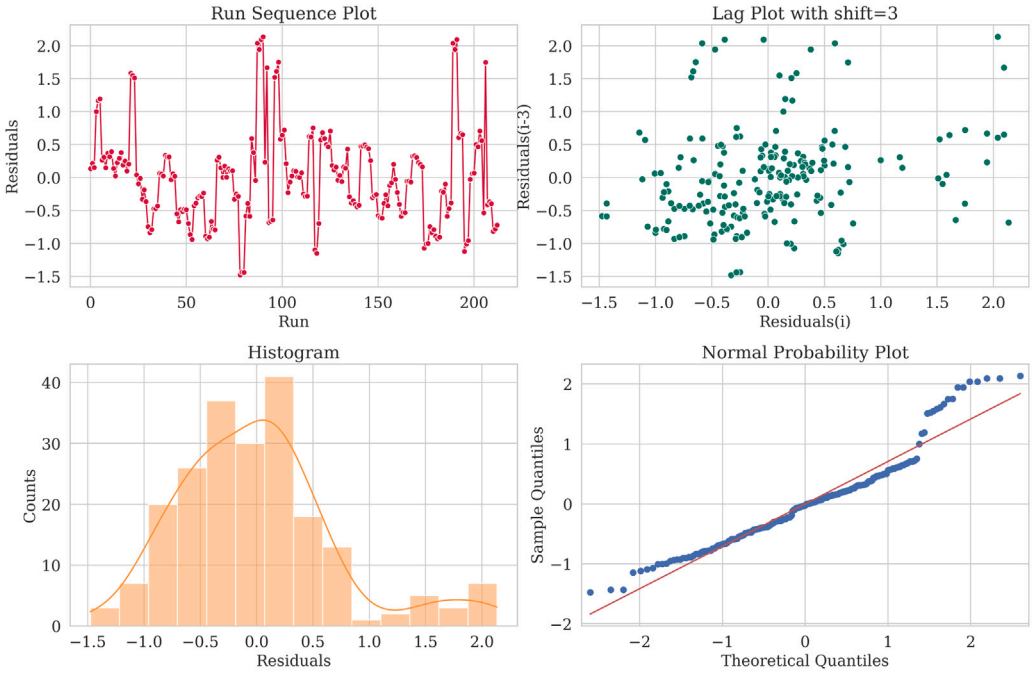

Fig. 15. 4-plot of the model's residual.

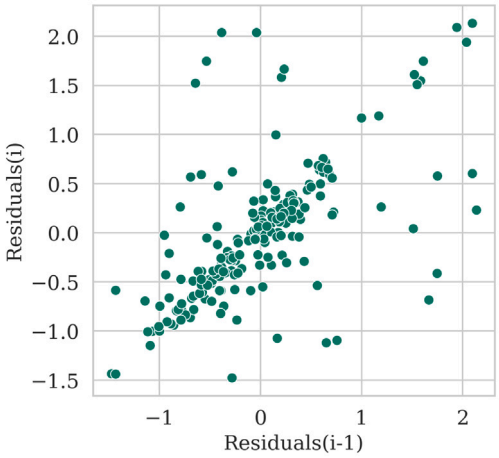

Fig. 16. Lag 1 plot.

Table 6
Model estimates in order of importance.

Coefficient	Value	Description
β_0		Intercept
β_A	−0.791	Air
β_{PG}	0.379	Position · Grid
β_{IW}	−0.302	Intrusion · Water
β_I	−0.246	Intrusion
β_{IA}	0.200	Intrusion · Air
β_{GA}	0.131	Grid · Air
β_{IG}	0.117	Intrusion · Grid
β_{WA}	−0.106	Water · Air
β_G	−0.050	Grid
β_{PI}	−0.044	Position · Intrusion
β_{PW}	0.036	Position · Water
β_P	0.023	Position
β_{PP}	−0.019	Position^2
β_{PA}	−0.019	Position · Air
β_{II}	0.018	Intrusion^2
β_{GW}	−0.015	Grid · Water
β_W	0.013	Water
β_{AA}	−0.002	Air^2
β_{GG}	0	Grid^2
β_{WW}	0	Water^2

of them covering a complementary section of the whole dataset. This approach was done for three different cases, in which the sub-groups were created as follows:

- Without/With the splashing Grid ($G = -1; G = 1$);
- Horizontal/Vertical inlet Position ($P = -1; P = 0, 1$);
- Without/With channels Intrusion ($I = -1; I = 0, 1$).

For each of these three cases, two different complementary models were developed. Their accuracy is shown in the bar plot in Fig. 17 in terms of R^2 of the corresponding regression model. For each case, one of the models gives good accuracy, but not the counterpart. This indicates that for specific conditions, high accuracy models could correctly predict the goodness of flow distribution. However, the process is too complex to be predicted by general models with all parameters unknown.

To test the regression models, 6 additional runs were performed and the predicted responses were compared to the real one. In Fig. 18 the real (blue) and predicted responses are compared: values closer to the blue curve are representative of better model accuracy. For the selected runs, the best model seems to be the one that splits the dataset based on the grid level (green line). However, these additional runs were used only to test the models. If these regressions are to be used in future works, the authors advise to look at the model's accuracy for the selection of the best one.

6. Conclusion

The present paper describes a methodology based on DoE techniques for the analysis of the flow phases distribution in the channels of an evaporator header. The main objective was to develop an approach for defining the experimental matrix and for analyzing the results. Such methodology was then applied to a specific case study, in order to capture and assess the effect of multiple parameters and their interactions on the goodness of the distribution. After choosing the factors

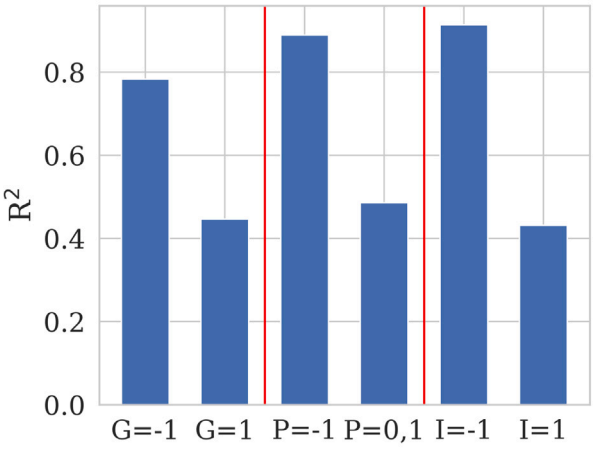

Fig. 17. Accuracy of the splitted models.

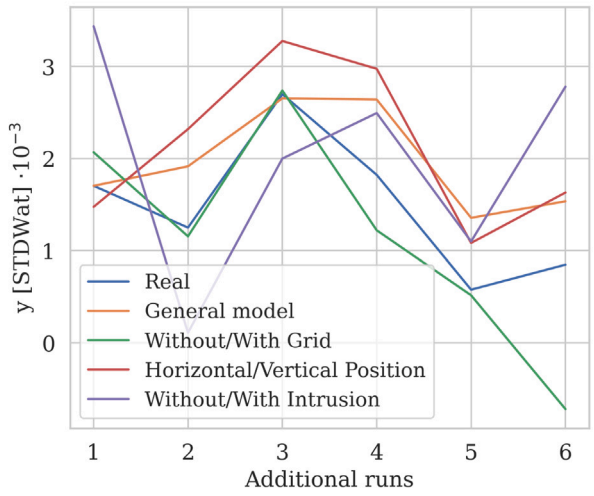

Fig. 18. Prediction of the response via the different developed models.

of interest to be tested, the DoE experimental matrix was defined by combining optimality criteria. A matrix with 72 runs was selected as it fell within the allowable time and resources available. The number of runs was thus decreased by 33% globally with respect to a Full Factorial. The major conclusions from the result analysis are reported herein:

1. For a correct prediction of the best combination of parameters, it is not sufficient to look at only Main Effects. Interaction effects are significant and cannot be neglected. This result was proven both graphically and analytically.
2. By analyzing all the interaction effects, the authors found two equally-best combinations of factor levels, both with the highest air flow rate (A = 1) (Table 5). The first one was experienced with horizontal inlet position (P = −1), without channel intrusion (I = −1), presence of the grid (G = 1), and lowest water flow rate (W = −1). The second one, instead, was given by central vertical inlet position (P = 1), highest channel intrusion (I = 1), without the splashing grid (G = −1), and highest air flow rate (A = 1). The visualization of water flow rate in the eight channels (Fig. 14) confirmed that the supposed best layout was indeed giving equal distribution across the channels. In addition, with only Main Effect analysis, an indication of a good layout can be obtained but it deviates from the best one. This was the graphical proof of the methodology's validity.
3. Having scaled all the factor levels between −1 and 1, we can have an idea of the most affecting parameters by looking at the DoE Mean (Fig. 7) and Interaction (Fig. 8) plots. For a quantification of the effects, we can compare the coefficient estimates of the model in Table 6. The 5 most affecting terms are, in order: Air, Position-Grid, Intrusion-Water, Intrusion, Intrusion-Air. Second order interactions are instead not significant: for our application, a model with main and interaction effects can be an alternative with similar accuracy and smaller complexity.
4. If we had looked at only Main Effects, we would have concluded that Grid and Water effects were not significant. Instead, their combination with other factors is highly affecting the response, being PG and IW the second and third most affecting terms.
5. A universal regression model of the phenomena has low accuracy (51%) and cannot be trusted to correctly predict the flow distribution. The presence of multi-phase flows increases the complexity, making it difficult to obtain a general equation capable of predicting the performances. This confirms what was found in the literature.
6. If one restricts the area of analysis, more specific models can be developed with narrower fields of study. This approach was followed with 3 different sub-groups of the whole dataset: with/without the presence of the splashing grid; with horizontal/vertical inlet position; with/without channels intrusion. For some cases, the accuracy of the sub-models is acceptable (Fig. 17) This indicates that, for specific conditions, high accuracy models could correctly predict the goodness of flow distribution: without the grid (accuracy 78.3%), with horizontal inlet (accuracy 88.9%) or without channels intrusion (accuracy 91.4%). However, as expected, a predictive model of the general phenomena is not easily obtainable except for specific cases. This happens due to the complexity of the flow phases distribution and the dependencies of numerous variables.

The results demonstrated that the developed methodology has strong potential to provide valuable insights into complex phenomena, such as those involving multi-phase flows. Even if the results presented are for a specific header-channels orientation, the approach can be applied with different header configurations and operating conditions: for each specific case, the response function, factors, and levels can be adjusted as necessary, while still following the outlined methodology. This flexibility makes the approach highly versatile and applicable to a wide range of engineering challenges, especially in areas involving multi-phase flows, where the combination of factors and levels has, until now, limited the use of existing DoE matrixes. These methods have the potential to provide significant support to researchers involved in experimental analysis.

The described methodology will be applied to another test case using the same experimental set-up, but with modified operating conditions to achieve flow similarity with low Global Warming Potential fluids, as well as changes to the tested parameters. Given that header-channel configurations are among the most influential variables, the authors plan to include them as a factor in the following campaign. This approach will give insights into the effect of factors interaction, which has never been explored in the state of the art, especially for low GWP fluids.

CRediT authorship contribution statement

Claretta Tempesti: Writing – review & editing, Writing – original draft, Validation, Methodology, Investigation, Data curation, Formal analysis, Visualization. **Aude Lecardonnel:** Writing – review & editing, Writing – original draft, Supervision, Data curation, Formal analysis. **Delphine Laboureur:** Writing – review & editing, Supervision, Conceptualization, Funding acquisition, Project administration.

Declaration of competing interest

The authors declare that they have no known competing financial interests or personal relationships that could have appeared to influence the work reported in this paper.

Acknowledgments

This project has received funding from the Clean Sky2 Joint Undertaking (JU), Belgium under grant agreement No 886698. The JU receives support from the European Union's Horizon 2020 research and innovation programme and the Clean Sky 2 JU members other than the Union, Belgium. This paper reflects only the author's view and that the JU is not responsible for any use that may be made of the information it contains.

Data availability

The authors do not have permission to share data.

References

[1] Julio C. Pacio, Carlos A. Dorao, A study of the effect of flow maldistribution on heat transfer performance in evaporators, Nucl. Eng. Des. (ISSN: 00295493) 240 (2010) 3868–3877, http://dx.doi.org/10.1016/j.nucengdes.2010.09.004.

[2] Martin Ryhl Kærn, Wiebke Brix, Brian Elmegaard, Lars Finn Sloth Larsen, Performance of residential air-conditioning systems with flow maldistribution in fin-and-tube evaporators, Int. J. Refrig. (ISSN: 01407007) 34 (2011) 696–706, http://dx.doi.org/10.1016/j.ijrefrig.2010.12.010.

[3] J. Choi, William Payne, Piotr Domanski, Effects of non-uniform refrigerant and air flow distributions on finned-tube evaporator performance, in: Refrigeration International Congress, 21st IIR. (IRC2003). 10th Technical Session Energy-Efficient Heating and Cooling Systems for Buildings, Proceedings. August 17-22, 2003 , Washington, DC, USA, 2003, URL https://tsapps.nist.gov/publication/get_pdf.cfm?pub_id=101203.

[4] E.R. Dario, L. Tadrist, J.C. Passos, Review on two-phase flow distribution in parallel channels with macro and micro hydraulic diameters: Main results, analyses, trends, Appl. Therm. Eng. (ISSN: 13594311) 59 (2013) 316–335, http://dx.doi.org/10.1016/j.applthermaleng.2013.04.060.

[5] Tong Xiong, Guoqiang Liu, Shenjie Huang, Gang Yan, Jianlin Yu, Two-phase flow distribution in parallel flow mini/micro-channel heat exchangers for refrigeration and heat pump systems: A comprehensive review, Appl. Therm. Eng. (ISSN: 13594311) 201 (2022) http://dx.doi.org/10.1016/j.applthermaleng.2021.117820.

[6] Nae-Hyun Kim, Tae-Ryong Sin, Two-phase flow distribution of air–water annular flow in a parallel flow heat exchanger, Int. J. Multiph. Flow 32 (12) (2006) 1340–1353.

[7] Nae-Hyun Kim, Do-Young Kim, Jin-Pyo Cho, Jung-Oh Kim, Tae-Kyun Park, Effect of flow inlet or outlet direction on air-water two-phase distribution in a parallel flow heat exchanger header, Int.J. Air-Cond. Refrig. 16 (2) (2008) 37–43.

[8] Nae-Hyun Kim, Ho-Won Byun, Refrigerant distribution in a minichannel evaporator having vertical headers, Heat Transfer Eng. 35 (11–12) (2014) 1105–1113.

[9] Yang Zou, Pega S. Hrnjak, Effects of fluid properties on two-phase flow and refrigerant distribution in the vertical header of a reversible microchannel heat exchanger–comparing R245fa, R134a, R410a, and R32, Appl. Therm. Eng. 70 (1) (2014) 966–976.

[10] Z.M. Razlan, S.A. Bakar, H. Desa, W.K. Wan, I. Zunaidi, I. Ibrahim, N.S. Kamarrudin, M.J.M. Ridzuan, K. Takiguchi, T. Tsuchiya, Y. Kitade, M. Hirota, N. Maruyama, A. Nishimura, Experimental study on gas–liquid flow distributions in upward multi-pass channels—Comparison of R-134a flow and air–water flow, Exp. Therm Fluid Sci. (ISSN: 08941777) 91 (2018) 134–143, http://dx.doi.org/10.1016/j.expthermflusci.2017.10.004.

[11] J.K. Lee, The effect of header and channel angle variation on two-phase flow distribution at multiple junctions, Korean J. Air-Cond. Refrig. Eng. 27 (11) (2015) 559–566.

[12] Jun Kyoung Lee, Sang Yong Lee, Distribution of two-phase annular flow at header–channel junctions, Exp. Therm. Fluid Sci. 28 (2–3) (2004) 217–222.

[13] J.K. Lee, Two-phase flow behavior inside a header connected to multiple parallel channels, Exp. Therm Fluid Sci. 33 (2009) 195–202.

[14] Jun Kyoung Lee, Optimum channel intrusion depth for uniform flow distribution at header-channel junctions, J. Mech. Sci. Technol. 24 (2010) 1411–1416.

[15] Jun Koung Lee, Study on effect of channel intrusion depth on the two-phase flow distribution at header-channel junction, Korean J. Air-Cond. Refrig. Eng. 28 (11) (2016) 444–449.

[16] E.R. Dario, L. Tadrist, J.L.G. Oliveira, J.C. Passos, Measuring maldistribution of two-phase flows in multi-parallel microchannels, Appl. Therm. Eng. 91 (2015) 924–937.

[17] P. Fei, P. Hrnjak, Adiabatic Developing Two-Phase Refrigerant Flow in Manifolds of Heat Exchangers, Air Cond. Refrig. Center TR-225 (2004).

[18] Mohammad Ahmad, Georges Berthoud, Pierre Mercier, General characteristics of two-phase flow distribution in a compact heat exchanger, Int. J. Heat Mass Transfer 52 (1–2) (2009) 442–450.

[19] Mark Anthony Redo, Jongsoo Jeong, Niccolo Giannetti, Koji Enoki, Seiichi Yamaguchi, Kiyoshi Saito, Hyunyoung Kim, Characterization of two-phase flow distribution in microchannel heat exchanger header for air-conditioning system, Exp. Therm Fluid Sci. (ISSN: 08941777) 106 (2019) 183–193, http://dx.doi.org/10.1016/j.expthermflusci.2019.04.021.

[20] David Schmid, Bart Verlaat, Paolo Petagna, Rémi Revellin, Jürg Schiffmann, Flow pattern observations and flow pattern map for adiabatic two-phase flow of carbon dioxide in vertical upward and downward direction, Exp. Therm Fluid Sci. (ISSN: 08941777) 131 (2022) http://dx.doi.org/10.1016/j.expthermflusci.2021.110526.

[21] Douglas C. Montgomery, Design and Analysis of Experiments, Wiley, ISBN: 9781118146927, 2012.

[22] Joon Hyung Kim, Him Chan Lee, Jin Hyuk Kim, Young Seok Choi, Joon Yong Yoon, Il Soo Yoo, Won Chul Choi, Improvement of hydrodynamic performance of a multiphase pump using design of experiment techniques, J. Fluids Eng. Trans. ASME (ISSN: 1528901X) 137 (2015) http://dx.doi.org/10.1115/1.4029890.

[23] Benedetto Bozzini, Marco E. Ricotti, Marco Boniardi, Claudio Mele, Evaluation of erosion-corrosion in multiphase flow via CFD and experimental analysis, Wear (ISSN: 00431648) 255 (2003) 237–245, http://dx.doi.org/10.1016/S0043-1648(03)00181-9.

[24] Azael Capetillo, Fernando Ibarra, Multiphase injector modelling for automotive SCR systems: A full factorial design of experiment and optimization, Comput. Math. Appl. (ISSN: 08981221) 74 (2017) 188–200, http://dx.doi.org/10.1016/j.camwa.2017.01.025.

[25] Taijong Sung, Daesik Oh, Sangrok Jin, Tae Won Seo, Jongwon Kim, Optimal design of a micro evaporator with lateral gaps, Appl. Therm. Eng. (ISSN: 13594311) 29 (2009) 2921–2926, http://dx.doi.org/10.1016/j.applthermaleng.2009.02.015.

[26] NIST/SEMATECH e-handbook of statistical methods, 2012, http://dx.doi.org/10.18434/M32189, http://www.itl.nist.gov/div898/handbook/. (Accessed 2021-10, 2021-12).

[27] Aleksandar Jankovic, Gaurav Chaudhary, Francesco Goia, Designing the design of experiments (DOE) – An investigation on the influence of different factorial designs on the characterization of complex systems, Energy Build. (ISSN: 03787788) 250 (2021) http://dx.doi.org/10.1016/j.enbuild.2021.111298.

[28] Angela Dean, Daniel Voss, Danel Draguljić, Springer Texts in Statistics Design and Analysis of Experiments Second Edition, Springer, 2017, URL http://www.springer.com/series/417.

[29] Peter Goos, Bradley Jones, Optimal design of experiment - A case study approach, John Wiley & Sons, Ltd, 2011, pp. i–xv, http://dx.doi.org/10.1002/9781119974017.fmatter,

[30] Ho-Won Byun, Nae-Hyun Kim, Effect of row-crossing header configuration on refrigerant distribution in a two row/four pass parallel flow minichannel heat exchanger, Int. J. Heat Mass Transfer 89 (2015) 124–137.

[31] M. Ahmad, G. Berthoud, P. Mercier, General characteristics of two-phase flow disitrbution in a compact heat exchanger, Int. J. Heat Mass Transfer 52 (2009) 442–450.

[32] Aude Lecardonnel, Delphine Laboureur, Piero Colonna, Two-phase flow metering of maldistribution inside a header by mean of venturi flowmeter solely, Multiphase Sci. Technol. (2024).

[33] Sebastian Haan, Doegen python package, 2021, https://pypi.org/project/DoEgen/. (Accessed 2021-11 2021-12).

[34] Nae Hyun Kim, Eul Jong Lee, Ho Won Byun, Two-phase refrigerant distribution in a parallel flow minichannel heat exchanger having horizontal headers, Int. J. Heat Mass Transfer (ISSN: 00179310) 55 (2012) 7747–7759, http://dx.doi.org/10.1016/j.ijheatmasstransfer.2012.07.082.

[35] Agung Tri Wijayanta, Takahiko Miyazaki, Shigeru Koyama, Refrigerant distribution in horizontal headers with downward minichannel-branching conduits: Experiment, empirical correlation and two-phase flow pattern map, Exp. Therm Fluid Sci. (ISSN: 08941777) 81 (2017) 430–444, http://dx.doi.org/10.1016/j.expthermflusci.2016.09.011.

[36] N.-H. Kim, D.-Y. Kim, H.-W. Byun, Effect of inlet configuration on the refrigerant distribution in a parallel flow minichannel heat exchanger, Int.J. Refrig. 34 (2011) 1209–1221.